ISSN 1022-8594
JUJS

Vol. 42, No. 1, pp. 83-101

Density Functional Theory Investigation on Electronic Structure, Photophysical Properties and Vibrational Spectra of Diphenylacetylene

Tahmina Haque and *Khurshida Khayer
Department of Chemistry, Jahangirnagar University, Savar, Dhaka-1342

Abstract

In the present work, the electronic UV-Vis spectra of diphenylacetylene were calculated by time dependent density functional theory (TD-DFT) computational method; their electronic transitions were analyzed and compared in gas phase and in ethanol solvent. ZIndo and CIS computational methods were also employed to compute the electronic transitions in gas phase. The ground state geometries were calculated by density functional theory (DFT) method using B3LYP functional with 6-31+G(d,p) basis set, ab *initio* HF/6-31G(d,p) and semi-empirical AM1 methods for diphenylacetylene in gas phase. The infrared and Raman scattering spectra, their intensities were calculated for diphenylacetylene by DFT-B3LYP/6-31+G(d,p) and HF/6-31G(d,p) method.

Keywords: Diphenylacetylene, DFT calculation, electronic transition, calculated UV-Vis and vibrational spectra, frontier molecular orbitals.

Introduction

The parent acetylene having a triple bond, substituted with two phenyl groups, named, diphenyl acetylene (DPA) and its derivatives, have attracted much attention not only for their high energy-efficiencies [1-4] in dendritic antenna molecules but also for their possible uses as molecular wires in molecular devices [5-6]. To understand the role played by the DPA moiety in these molecular photonics, it is necessary to understand and investigate the structure and dynamics of both the ground and excited electronic states. During the past decade, the different quantum mechanical methods especially density functional theory [7] has emerged as a powerful tool to study the structural behavior and gain insight into the electronic structure *e.g.*, electronic transitions and transition probability, UV-Vis spectra, Frontier molecular orbitals (FMOs) and their energies, HOMO-LUMO gap, vibrational frequencies and spectra, *etc.* of medium sized and fairly large molecules. The main objective of the present study is to investigate the structural and electronic properties of DPA by means of

*Author for correspondence e-mail: khurshida_k_chem@yahoo.com

quantum mechanical calculations with the density functional theory (DFT), *ab initio* Hartree-Fock (HF) and semi-empirical AM1 method.

Computational Methods

All the quantum chemical calculations were carried out using the Gaussian 16W Rev: A.03 program [8]. The molecular structure and energies of diphenylacetylene (DPA) were computed employing the quantum chemical methods, *e.g.*, density functional theory (DFT) method using B3LYP (Becke-3-Lee-Yang-Parr) functional [9] with 6-31+G(d,p) basis set, *ab initio* Hartree Fock and semi-empirical AM1 [10]. The obtained optimized parameters were used to calculate the vibrational frequencies at the same level of theory. The Raman and infrared intensities were calculated by the harmonic approximations at the same level of theory used for the optimized geometries. All the ground state geometries were found as the true minima since negative vibrational frequencies were absent in all cases. DFT method was also employed to calculate the optimized electronic structure in ethanol solvent. Time dependent density functional theory, TD-DFT method [11] was employed to calculate the electronic transitions both in the gas phase and ethanol solvent. TD-DFT calculations using the hybrid functional B3LYP with 6-31+G(d,p) basis set were carried out on the 20 lowest spin allowed singlet-singlet transitions for DPA in gas phase and ethanol solvent.

Results and Discussion

Electronic Structure and Geometry. Figure 1 shows the calculated ground state electronic structure with the atom numbering of diphenylacetylene (DPA) in gas phase at DFT level of theory using B3LYP functional with 6-31G+(d,p) basis set. The ground state structure calculated at the same level of theory in ethanol solvent is also shown in the Figure 1. The ground state optimized geometries of DPA having planar form (D_{2h} symmetry) calculated by different quantum chemical methods, *e.g.*, semi-empirical AM1, *ab initio* Hartree Fock (HF)/6-31G(d,p) and density functional theory DFT-B3LYP/6-31+G(d,p) both in the gas phase and ethanol solvent are respectively presented in Table 1. All the optimized ground state geometries were verified by vibrational frequency analysis at the respective same level of theory and found as

true minima since no imaginary frequencies were found in all the cases. The geometry parameters calculated by semi-empirical AM1 for DPA (Table 1) is well agreed with the earlier reported theoretical work [12] and reported experimental work as discussed below. The central $C_1 \equiv C_2$ triple bond length (1.1999 Å) of our calculated AM1 method reproducible with the work of Palafox [12] (1.1999 *vs*. 1.2000 Å), and fairly matches with the work of Attila *et al* [13] and Shimojima *et al* [14] by *ab initio* 4-31G calculation (1.1999 *vs* 1.194 Å) and by XRD (1.1999 *vs*. 1.198 Å). The present calculated planar DPA (D_{2h} symmetry) is same as reported X-ray crystal [15] and electron diffraction structure in the gas phase. The energies of the DPA in gas phase and ethanol are -539.498490 a.u. and -539.503750 a.u., respectively. The energy difference between them is found 3.30 kcal/mol.

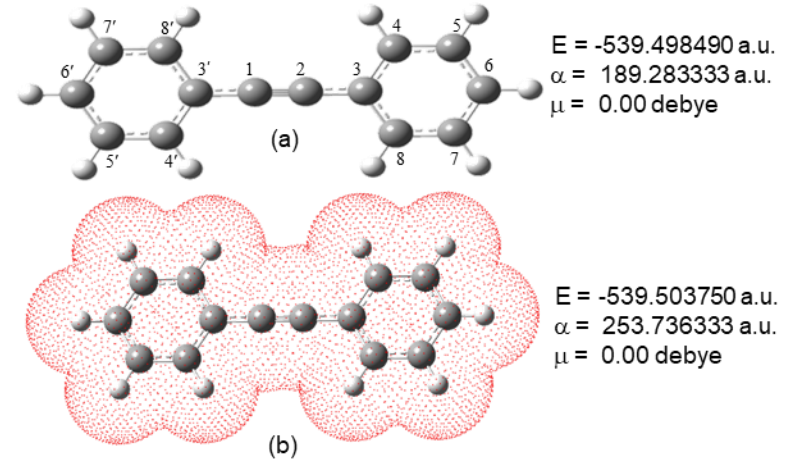

Figure 1: (a) Ground state optimized geometry of DPA calculated at DFT-B3LYP/6-31+G(d,p) method in gas phase, and (b) polarize continuum model cavity image of DPA calculated at DFT-B3LYP/6-31+G(d,p) method in ethanol; (E) energies, (μ) dipole moment and (α) polarizability.

An insignificant structural change of DPA geometry in ethanol solvent was observed. The central carbon carbon triple bond length is longer in ethanol. The other bond lengths are also found as longer values though in very

small scale. The bond angles $\angle C_8–C_3–C_4$ and $\angle C_{8'}–C_{3'}–C_{4'}$ deviates only 0.5^o.

It should be noted that the perpendicular form of diphenylacetylene having D_{2d} symmetry produces different optimized geometries with very low negative frequencies (-7.64, -3.89, and -21.58 cm^{-1}) by AM1, HF/6-31+G(d,p) and DFT-B3LYP/6-31+G(d,p) methods respectively. As the structures show negative frequencies, their optimized structures (perpendicular form, D_{2d} symmetry) are not considered in the present work as ground state structure. However, the planar form was found as more stable than the perpendicular one by only 0.22 kcal/mol, 0.37 kcal/mol and 0.77 kcal/mol calculated by our semi-empirical AM1, HF/6-31+G(d,p) and DFT-B3LYP/6-31+G(d,p) methods, respectively.

Table 1. Optimized geometric parameters[a] of DPA in the ground state calculated at semi-empirical AM1, HF/6-31G(d,p) and DFT-B3LYP/6-31+G(d,p) methods in gas phase and ethanol solvent.

Parameters[a]	DPA			
	AM1	HF[b,c]	DFT[d]	DFT[e]
$C_1≡C_2$	1.1999	1.192	1.218	1.219
$C_2–C_3$	1.406	1.440	1.427	1.428
$C_1–C_{3'}$	1.406	1.440	1.427	1.428
$C_3–C_4$	1.405	1.394	1.410	1.412
$C_4–C_5$	1.393	1.383	1.394	1.395
$C_5–C_6$	1.395	1.386	1.399	1.400
$C_6–C_7$	1.395	1.386	1.399	1.400
$C_7–C_8$	1.393	1.383	1.394	1.395
$C_8–C_3$	1.405	1.394	1.410	1.412
$C_{3'}–C_{4'}$	1.405	1.394	1.405	1.412
$C_{4'}–C_{5'}$	1.393	1.383	1.393	1.395
$C_{5'}–C_{6'}$	1.395	1.386	1.395	1.400
$C_{6'}–C_{7'}$	1.395	1.386	1.395	1.400
$C_{7'}–C_{8'}$	1.393	1.394	1.393	1.395
$C_{8'}–C_{3'}$	1.405	1.394	1.405	1.412
$C_4–H$	1.099	1.075	1.085	1.085
$C_5–H$	1.100	1.075	1.086	1.086
$C_6–H$	1.099	1.075	1.086	1.086
$C_7–H$	1.100	1.075	1.086	1.086
$C_8–H$	1.099	1.075	1.085	1.085

$C_{4'}$–H	1.099	1.075	1.085	1.085
$C_{5'}$–H	1.100	1.075	1.086	1.086
$C_{6'}$–H	1.099	1.075	1.086	1.086
$C_{7'}$–H	1.100	1.075	1.086	1.086
$C_{8'}$–H	1.099	1.075	1.085	1.085
$\angle C_{3'}$–$C_1 \equiv C_2$	180.0	180.0	180.0	180.0
$\angle C_1 \equiv C_2$–C_3	180.0	180.0	180.0	180.0
$\angle C_3$–C_4–C_5	120.1	120.3	120.6	120.3
$\angle C_4$–C_5–C_6	120.3	120.2	119.6	120.3
$\angle C_5$–C_6–C_7	119.9	119.8	120.2	119.8
$\angle C_6$–C_7–C_8	120.3	120.2	119.6	120.3
$\angle C_7$–C_8–C_3	120.1	120.3	120.6	120.3
$\angle C_8$–C_3–C_4	119.4	119.2	119.4	118.9
$\angle C_8$–C_3–C_2	120.3	120.4	120.5	120.5
$\angle C_4$–C_3–C_2	120.3	120.4	120.5	120.5
$\angle C_{3'}$–$C_{4'}$–$C_{5'}$	120.1	120.3	120.0	120.3
$\angle C_{4'}$–$C_{5'}$–$C_{6'}$	120.3	120.2	120.3	120.3
$\angle C_{5'}$–$C_{6'}$–$C_{7'}$	119.9	119.8	119.9	119.8
$\angle C_{6'}$–$C_{7'}$–$C_{8'}$	120.3	120.2	120.3	120.3
$\angle C_{7'}$–$C_{8'}$–$C_{3'}$	120.1	120.3	120.0	120.3
$\angle C_{8'}$–$C_{3'}$–$C_{4'}$	119.4	119.2	119.4	118.9
$dAC_{3'}$–$C_1 \equiv C_2$–C_3	∞	∞	∞	∞

[a]Bond lengths in angstroms, bond angles, ∠ and dihedral angles, dA in degrees. [b]HF/6-31G(d,p). [c]HF/6-31+G(d,p) produces insignificant changes, hence data are not shown. [d]DFT-B3LYP/6-31+G(d,p) in gas phase . [e]DFT-B3LYP/6-31+G(d,p) in ethanol solvent.

UV-Vis Spectra and Electronic Transition

The UV-Vis spectra of DPA calculated by time dependent density functional theory (TD-DFT) method from optimized geometry of DPA calculated at DFT level of theory using the B3LYP functional and 6-31+G(d,p) basis set in gas phase and in ethanol solvent are shown in Figure 2 and the optical data are presented in Table 2.

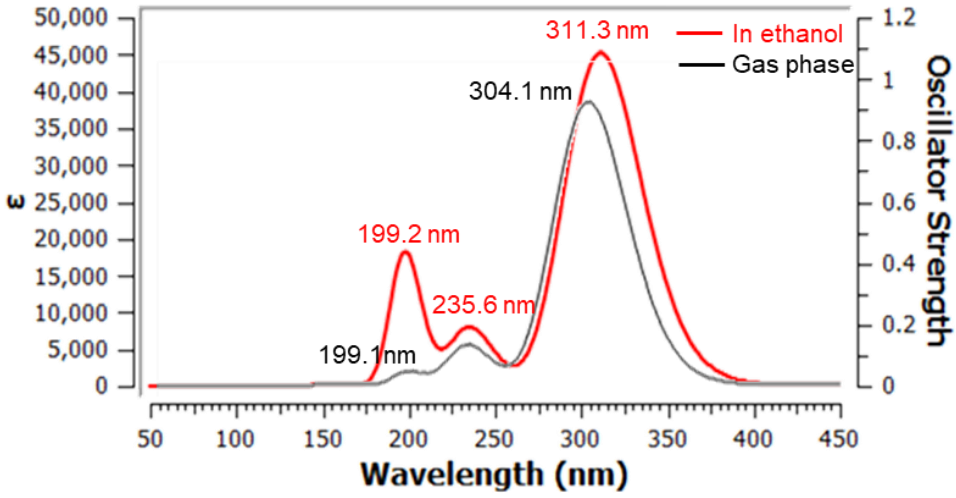

Figure 2: The electronic UV-Vis spectra of DPA calculated at TD-DFT//DFT-B3LYP/6-31+G(d,p) in gas phase and ethanol solvent.

The calculated electronic UV-Vis spectra (Figure 2) of DPA in gas phase exhibits a characteristic broad and large band centered at λ_{max} 304.1 nm with large oscillator strength (f = 0.9481) corresponding to HOMO-LUMO transition (Figure 5) of π–π* transition and large extinction co-efficient (ε_{max} 3.7 × 10^4 M^{-1} cm^{-1}). Other two bands with lower band intensity centered at λ_{max} 234.3 nm (ε_{max} 5.0 × 10^3 M^{-1} cm^{-1}) and λ_{max} 199.1 nm (ε_{max} 500 M^{-1} cm^{-1}) with the oscillator strength of f = 0.1329 and f = 0.0389, respectively, are observed for π–π* transitions as well. The electronic transitions, absorption wavelength λ_{max} (nm), vertical excitation energies E_x (eV), and oscillator strength (f) are shown in Tables 2-3 calculated by different theoretical approach.

Table 2: Electronic transitions, absorption wavelength λ_{max} (nm), excitation energy E_x (eV), and oscillator strength (f) of DPA calculated at TD-DFT method.

Excited state	TD/DFT[a]			TD/DFT[b]		
	λ_{max} (f)	E_x	Sym.	λ_{max} (f)	E_x	Sym.
1	304.1 (0.9481)	4.08	B1U	311.3 (1.1140)	3.98	B1U
2	269.0 (0.0011)	4.61	B2U	267.9 (0.0001)	4.63	B2U
3	267.1 (0.0)	4.64	B3G	266.1 (0.0)	4.66	B3G

4	261.6 (0.0)	4.74	AU	258.8 (0.0)	4.69	AU
5	238.6 (0.0)	5.20	AG	237.7 (0.0)	5.22	AG
6	234.3 (0.1329)	5.29	B2U	235.6 (0.1927)	5. 26	B2U
7	233.6 (0.0)	5.31	B3G	234.6 (0.0)	5.28	B3G
8	233.0 (0.0020)	5.32	B3U	226.3 (0.0021)	5.48	B3U
9	221.0 (0.0)	5.61	B2G	218.3 (0.0)	5.70	AG
10	216.9 (0.0)	5.72	AG	214.0 (0.0)	5.79	AU
11	214.1 (0.0)	5.79	AU	210.9 (0.0)	5.88	B2G
12	210.5 (0.0)	5.89	B1G	202.1 (0.0)	6.13	B1G
13	206.4 (0.0062)	6.01	B3U	199.67 (0.0022)	6.21	B3U
14	202.9 (0.0015)	6.11	B3U	199.66 (0.0)	6.21	B3G
15	201.2 (0.0)	6.16	B2G	199.2(0.1476)	6.23	B1U
16	199.7 (0.0)	6.21	B3G	199.1 (0.0064)	6.23	B2U
17	199.3 (0.0)	6.22	AU	198.6 (0.0)	6.24	AG
18	199.2 (0.0015)	6.22	B2U	198.5 (0.0)	6.25	B3U
19	199.1 (0.0389)	6.23	B1U	198.0 (0.0)	6.26	B2G
20	198.83 (0.0)	6.24	AG	197.3 (0.2875)	6.29	B1U

[a]TD-DFT calculation from DFT-B3LYP/6-31+G(d,p) initial optimized geometry in gas phase. [b]TD-DFT calculation from DFT-B3LYP/6-31+G(d,p) initial optimized geometry in ethanol.

The solvent effect was considered in order to see whether the excited states can influence the excitation energy and intensity of the electronic transitions in DPA. The present UV-Vis spectral analysis shows that the incorporation of solvent shifts the absorption wavelength towards longer wavelength and larger extinction co-efficient. The UV-Vis spectrum of DPA in ethanol solvent possesses λ_{max} at 311.3 nm, red shifted (7.2 nm) compared to that of gas phase (λ_{max} 304.1 nm) with much higher ε_{max} 4.5×10^4 M^{-1} cm^{-1}. The band at 234.3 nm (gas phase) shifted to 235.6 nm showing a red shift (1.3 nm) with comparatively higher extinction co-efficient (Figure 2) in ethanol. The order of the excited state level with respect to π–π^* transition in different methods and both in the ethanol solvent and in gas phase is not found as exactly the same level in all cases (Table 2 & 3).

The electronic UV-Vis spectra of DPA by ZIndo and CIS method from semi-empirical AM1 and *ab initio* HF/6-31G(d,p) optimized geometries in gas phase respectively are shown in Figure 3 and presented at Table 3. Though the transition presents a large oscillator strength (f = 0.6211) in

accordance with the extinction co-efficient calculated at 327.5 nm (ε_{max} 2.5 × 10^4 M^{-1} cm^{-1}) for DPA by ZIndo method, a much higher absorption band was centered at 213.1 nm with extinction co-efficient of >9.0 × 10^4 M^{-1} cm^{-1}.

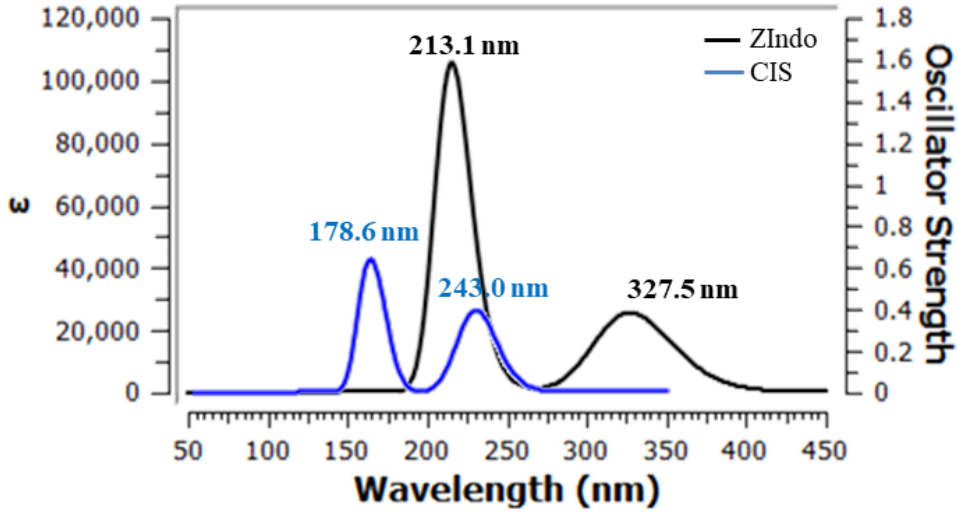

Figure 3: The electronic UV-Vis spectra of DPA by ZIndo and CIS from semi-empirical AM1 and *ab initio* HF/6-31G(d,p) optimized geometry, respectively in gas phase.

Table 3: Electronic transitions, absorption wavelength, λ_{max} (nm), excitation energy, E_x (eV), and oscillator strength (f) of DPA calculated at ZIndo, CIS and TD-DFT[c] method.

Excited state	ZIndo[a]		CIS[b]		TD/DFT[c]	
	λ_{max} (f)	E_x	λ_{max} (f)	E_x	λ_{max} (f)	E_x
1	338.7 (0.0)	3.66	242.97 (0.8460)	5.10	288.7 (0.9335)	4.29
2	327.5 (0.6211)	3.79	210.93 (0.0002)	5.88	260.0 (0.0014)	4.77
3	283.0 (0.0121)	4.38	209.80 (0.0)	5.91	258.1 (0.0)	4.80
4	282.9(0.0)	4.38	203.90 (0.0)	6.08	247.60 (0.0)	5.01
5	270.9 (0.0)	4.58	200.27 (0.0)	6.19	231.08 (0.0)	5.37
6	247.1 (0.0)	5.02	197.65 (0.0)	6.27	228.81 (0.0022)	5.42
7	234.3 (0.1679)	5.29	188.80 (0.0)	6.57	227.13 (0.1307)	5.46
8	222.1 (0.0)	5.58	181.25 (0.0)	6.84	226.39 (0.0)	5.48
9	222.0 (0.0)	5.58	178.91 (0.0)	6.93	217.09 (0.0)	5.71

10	218.8 (1.0116)	5.67	178.62 (0.7138)	6.94	211.94 (0.0)	5.85
11	213.1 (1.6353)	5.82	175.28 (0.0391)	7.07	206.92 (0.0)	5.99
12	211.3 (0.0)	5.87	171.70 (0.0)	7.22	203.07 (0.0)	6.11
13	210.0 (0.0)	5.90	170.86 (0.0)	7.26	202.98 (0.0067)	6.11
14	197.8 (0.0)	6.27	168.54 (1.0050)	7.36	197.30 (1.0016)	6.28
15	197.6 (0.0025)	6.28	167.62 (0.0)	7.40	196.74 (0.0)	6.30
16	196.8 (0.0)	6.30	166.29 (0.0)	7.46	196.19 (0.0011)	6.32
17	195.2 (0.0011)	6.35	165.18 (0.0)	7.51	196.07 (0.0378)	6.32
18	193.0 (0.0)	6.43	163.77 (0.0)	7.57	195.88 (0.0)	6.33
19	191.2 (0.0)	6.48	161.56 (0.0367)	7.67	195.63 (0.0)	6.34
20	183.6 (0.0)	6.75	158.77 (0.0417)	7.81	195.19 (0.0)	6.35

[a]ZIndo calculation from semi-empirical AM1 initial geometry. [b]CIS calculation from HF/6-31G(d,p) initial optimized geometry. [c]TD-DFT calculation from HF/6-31+G(d,p) initial geometry in gas phase.

The electronic transitions were calculated at the TD-DFT//DFT-B3LYP/6-31+G(d,p) level of theory in gas phase and in ethanol solvent. The frontier molecular orbitals (FMO) *e.g.,* highest occupied molecular orbital (HOMO), lowest unoccupied molecular orbital (LUMO) *etc.*, involved in the electronic transitions of DPA (Figures 4-5) are generated at the TD-DFT//DFT-B3LYP/6-31+G(d,p) level of theory. The different electron charge transfer pathways *viz.* HOMO→LUMO, HOMO–1→LUMO, HOMO–1→LUMO +1 *etc*. are shown in Figures 4-7. The electron density surfaces are presented in green and pink color drawn at 0.02 [e $bohr^{-3}$]$^{1/2}$ isodensity level. The excited states are represented by the bold corresponding numbers. The electronic transitions with only higher contributions (C%) of molecular orbitals are presented in Figures 4-7. The energy gap (Eg) between HOMO→LUMO and others are presented in Figures 4, 5, 6 and 7 respectively. In gas phase the HOMO → LUMO transition predicted at 304.1 nm with the oscillator strength (f = 0.9481) having 97 % transition probability while HOMO → LUMO transition predicted at 311.3 nm with the oscillator strength (f = 1.1140) having 98 % transition probability in the solvent phase (ethanol) are shown in Figures 4-5. The electronic transitions and involved molecular orbitals calculated at the ZIndo and CIS level of theory in gas phase are shown in Figures 6-7 and the different optical data are tabulated in Table 3.

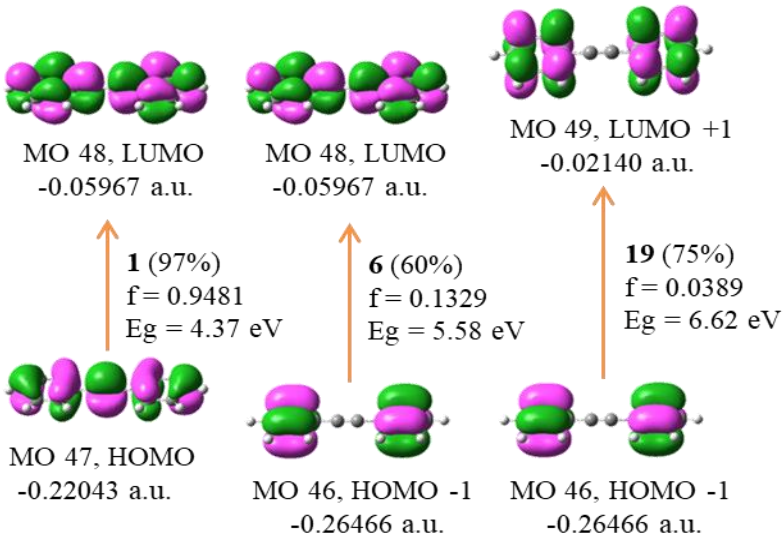

Figure 4: FMO orbitals (isovalue:0.02) [e bohr^{-3}]$^{1/2}$ of DPA from TD-DFT method in gas phase calculation. Green and pink color depicts different phases.

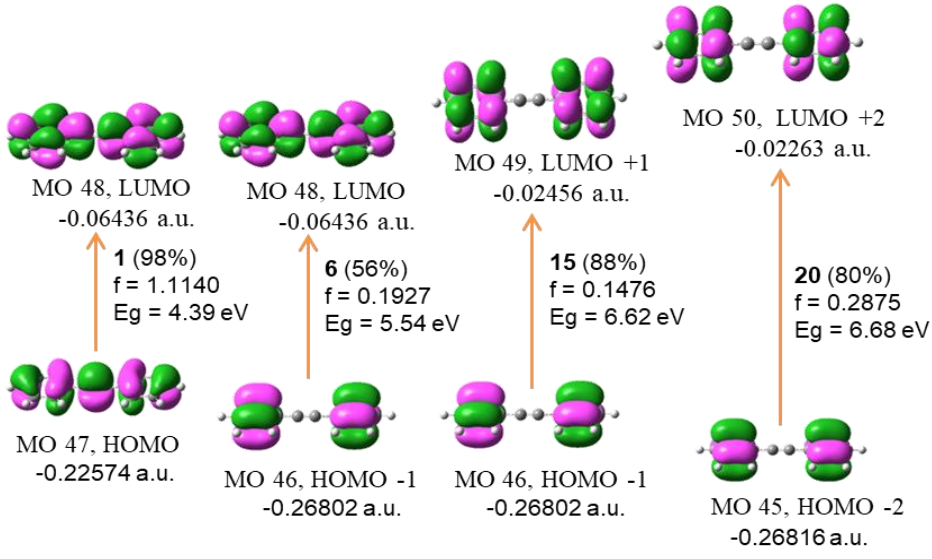

Figure 5: FMO orbitals (isovalue:0.02) [e bohr^{-3}]$^{1/2}$ of DPA from TD-DFT method in ethanol phase calculation. Green and pink color depicts different phases.

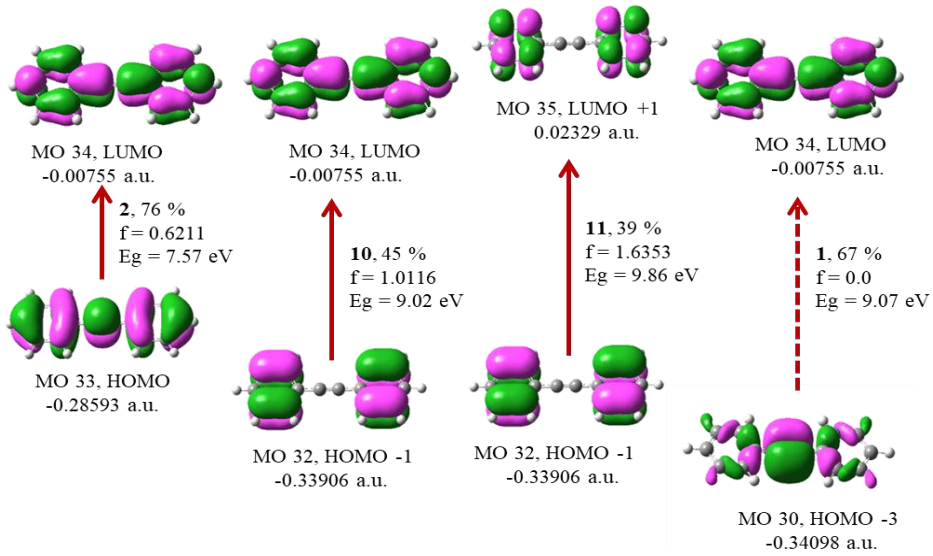

Figure 6: FMO orbitals (isovalue:0.02) [e bohr^{-3}]$^{1/2}$ of DPA from ZIndo method. Green and pink color depicts different phases.

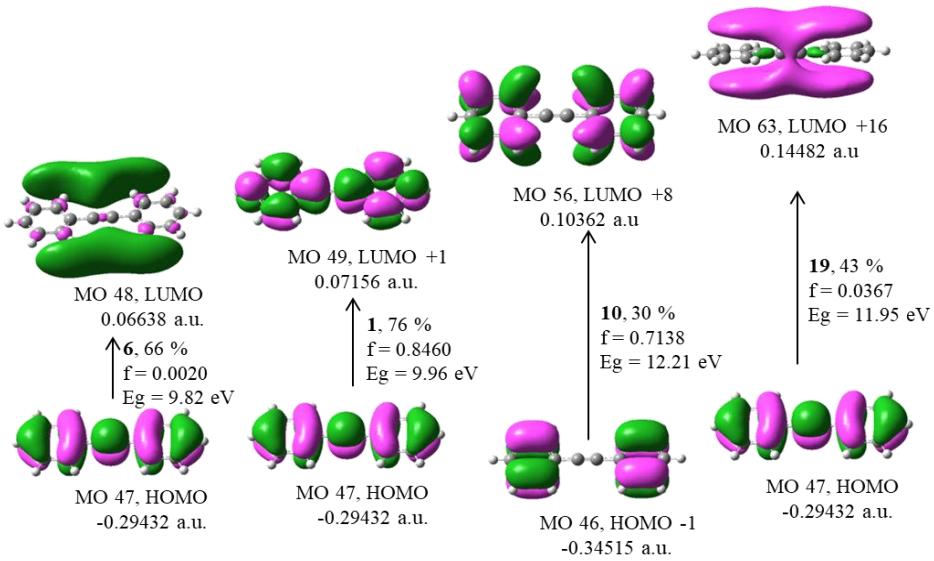

Figure 7: FMO orbitals (isovalue:0.02) [e bohr^{-3}]$^{1/2}$ of DPA from CIS method. Green and pink color depicts different phases.

Vibrational Spectra, Frequencies and Intensities:

The calculated vibrational spectra, frequencies (unscaled frequencies) and intensities of DPA by our DFT, HF, and semi-empirical AM1 (only frequencies) methods in the gas phase are shown in the Figures 8-10 and Table 4 respectively. The vibrational frequency of the central $C_1 \equiv C_2$ bond at 2494.59 cm^{-1} by our semi-empirical AM1 calculation matches with the earlier reported work [12]. The vibrational frequencies of the C=C, C-H and other modes is well matched with the reported work [12] as well with only a few exceptions by semi-empirical AM1 method. Though the vibrational frequency of the central $C_1 \equiv C_2$ bond by our semi-empirical AM1 calculation (Figure 8a) shows zero intensity at 2494.59 cm^{-1} the vibrational band is clearly shown in the Raman scattering spectra (Figure 8b). As for our DFT-B3LYP/6-31+G(d,p) calculation, the $C_1 \equiv C_2$ triple bond stretching vibration appears as zero intensity band at 2301.53 cm^{-1} (Figure 9a) whereas it appears as strong and polarized Raman scattering band (9373.64 A^4/AMU) at 2301.53 cm^{-1} (Figure 9b) in gas phase. In *ab initio* Hartree-Fock, HF/6-31G(d,p) calculation, the $C_1 \equiv C_2$ triple bond stretching vibration appears as zero intensity band at 2528.31 cm^{-1} (Figure 10a) whereas it appears as strong and polarized Raman scattering band (4610.84 A^4/AMU) at 2528.31 cm^{-1} (Figure 10b). It is clearly observed that Raman scattering spectra can be a useful tool to determine the vibrational spectra for symmetrically substituted acetylene derivative. The above Table 4 shows the computed vibrational frequency results of DPA in ethanol solvent as well. The peaks fall in the same order as in the gas phase. The values in the Table 4 indicate that the peak location for mode 56, the $C_1 \equiv C_2$ triple bond stretching vibration as for example in the IR spectrum is shifted to 6 cm^{-1} lower frequency (2301.53 cm^{-1} *vs.* 2295.35 cm^{-1}) in ethanol solvent with respect to the gas phase.

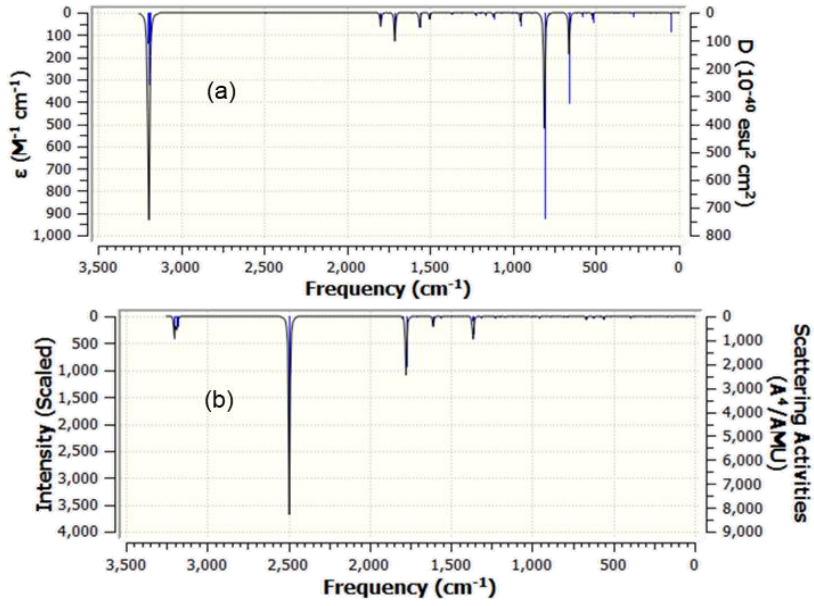

Figure 8: Electronic (a) IR (b) Raman scattering spectra of DPA by semi-empirical AM1 method.

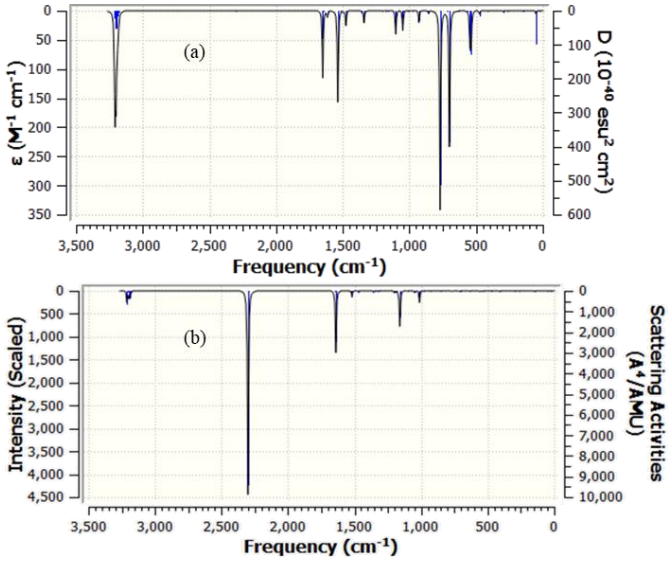

Figure 9: Electronic (a) IR (b) Raman scattering spectra of DPA by DFT-B3LYP/6-31+G(d,p) method.

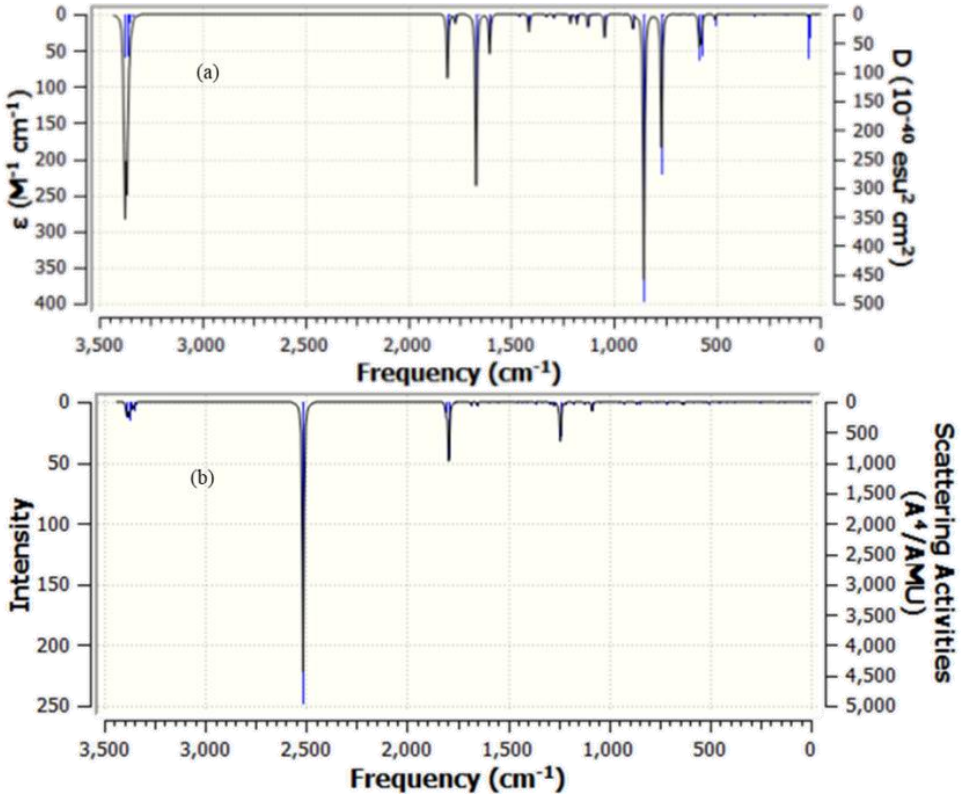

Figure 10: Electronic (a) IR and (b) Raman scattering spectra of DPA by HF/6-31G (d,p) method.

Table 4. Calculated vibrational frequencies of DPA with HF[a] and DFT[b,c] method in the ground state.

mode no.	AM1	HF			DFT					approximate description of mode[g] & [contribution of internal co-ordinates][h]
					In gas phase			In ethanol		
	Freq[d]	Freq[d]	I_{IR}[e]	I_{Raman}[f]	Freq[d]	I_{IR}[e]	I_{Raman}[f]	Freq[d]	I_{IR}[e]	
1	7.08	20.01	0.0000	0.0000	21.20	0.0000	0.0000	20.06	0.0000	twist (one ph ring wrt other); {$C_4C_3C_{3'}C_{8'}$ [24.2]}, {$C_4C_3C_{3'}C_{4'}$ [24.2]}, {$C_8C_3C_{4'}C_{3'}$ [24.2]}, {$C_8C_3C_{3'}C_{8'}$ [24.2]}
2	53.05	51.97	0.4920	0.0000	46.52	0.5562	0.0000	45.63	1.2101	sci. (one Ph ring wrt other)
3	54.58	57.36	1.0845	0.0000	53.26	1.2876	0.0000	51.48	2.2563	wag (one ring edge wrt other, -$C_1{\equiv}C_2$ -)
4	136.81	157.57	0.0000	5.6386	144.97	0.0000	2.2230	143.45	0.0000	twist (one ring wrt other, -$C_1{\equiv}C_2$ -)
5	172.08	174.52	0.0000	4.6054	148.70	0.0000	6.6983	149.42	0.0000	roc (both the ring, defm -$C_1{\equiv}C_2$ -)
6	277.43	274.02	0.0000	0.3961	259.69	0.0000	0.2655	259.38	0.0000	breathing (both ring,sym), str (half molecule wrt other)
7	302.23	319.28	0.1660	0.0000	295.62	0.2977	0.0000	294.70	0.5573	wag (-$C_1{\equiv}C_2$ -, one ring wrt other)
8	369.83	450.80	0.0000	0.0000	409.70	0.0000	11.8288	410.08	0.0000	twist (-$C_1{\equiv}C_2$ -, one ring wrt other)
9	369.98	452.60	0.0000	0.0482	411.26	0.0000	0.0000	411.18	0.0000	twist (ring)
10	393.05	455.14	0.0000	16.3836	413.67	0.0000	0.0025	412.29	0.0000	twist (ring)
11	519.41	510.07	2.2023	0.0000	474.06	1.5691	0.0000	473.25	3.1522	roc (each ring), defm - $C_1{\equiv}C_2$ -
12	524.25	576.79	10.238	0.0000	536.75	16.956	0.0000	535.28	27.29	wag (both the ring except C_1, C_4-H and $C_{1'}$, $C_{4'}$-H)
13	558.87	585.65	11.479	0.0000	545.99	15.899	0.0000	544.65	27.23	breathing (both ring, asym), str (C-$C_1{\equiv}C_2$ –C)
14	585.21	637.61	0.0000	53.9962	547.57	0.0000	10.9498	547.78	0.0000	twist {$C_{3'}C_1C_2$, $C_3C_2C_1$}, defm 4 C-C-C [8.0]; defm 4 C-C-H [17.6], C-C [3.0]
15	621.68	641.26	0.0000	21.2014	562.41	0.0000	23.3893	562.90	0.0000	twist (-$C_1{\equiv}C_2$ -), wag (each half DPA), twist wrt one another
16	659.16	680.85	0.0022	0.0000	633.48	0.0010	0.0000	631.40	0.0727	defm C-C-C
17	662.59	693.75	0.0000	1.2355	636.58	0.0000	6.5547	634.85	0.0000	defm C-C-C
18	666.61	762.88	0.0000	13.9829	699.28	0.0000	0.0722	698.60	0.0000	twist (ring C-H wrt one another)
19	667.64	768.34	0.0000	9.1400	700.49	67.317	0.0000	699.28	110.65	wag (ring C-H wrt one another)
20	787.11	769.16	53.145	0.0000	713.55	0.0000	14.6591	711.35	0.0000	breathing both ring
21	810.34	854.32	106.05	0.0000	765.73	0.0000	17.5739	764.69	0.0000	asym wag (C-H) wrt other ring

22	811.73	855.64	0.0000	8.4025	770.16	98.838	0.0000	769.17	152.69	sym wag (C-H) wrt other ring
23	887.93	909.69	5.2469	0.0000	853.08	0.0000	0.0000	853.25	1.6401	asym twist (C-H) wrt other ring
24	888.36	954.17	0.0000	0.0000	853.44	0.0000	0.9558	853.72	0.0000	sym twist (C-H) wrt other ring
25	954.86	954.83	0.0000	7.0220	856.13	1.2380	0.0000	854.14	0.0000	breathing wrt other ring
26	956.31	1044.98	0.0000	12.1977	927.44	0.0000	0.0000	931.64	0.0000	twist (each ring C-H + wrt one another)
27	960.06	1045.86	9.3862	0.0000	929.31	5.8126	0.0000	932.83	9.7968	twist (each ring C-H)
28	987.68	1088.01	0.0193	0.0000	981.96	0.0000	0.0000	987.86	0.0000	twist (each ring C-H)
29	987.93	1088.14	0.0000	172.9129	982.14	0.0000	0.0100	987.90	0.0000	twist (each ring C-H)
30	1006.54	1102.07	0.0000	0.0000	1001.69	0.0000	2.6485	1008.34	0.0000	twist (each ring C-H)
31	1006.66	1102.29	0.0000	0.0210	1001.79	0.0309	0.0000	1008.37	0.0450	twist (each ring C-H)
32	1072.85	1123.97	0.0000	26.0180	1011.79	0.0000	403.094	1008.89	0.0000	sym ring breathing wrt each other:{$C_3C_4C_5$ [3.0], $C_4C_5C_6$ [3.2], $C_5C_6C_7$ [3.1], $C_6C_7C_8$ [3.2], $C_3C_8C_7$ [3.0], $C_4C_3C_8$ [2.7]}
33	1118.98	1124.56	0.0000	5.6224	1011.89	0.0033	0.0000	1009.32	0.0000	asym ring breathing wrt each other:{$C_3C_4C_5$ [3.1], $C_4C_5C_6$ [3.3], $C_5C_6C_7$ [3.2], $C_6C_7C_8$ [3.3], $C_3C_8C_7$ [3.1], $C_4C_3C_8$ [2.9]}
34	1163.04	1124.58	0.1895	0.0000	1047.52	0.0000	56.6738	1044.39	0.0000	defm C-C-C, roc C-H
35	1164.08	1127.20	5.0736	0.0000	1050.02	9.7433	0.0000	1047.19	21.7005	defm C-C-C, roc C-H
36	1171.59	1179.49	0.0000	5.0966	1101.25	0.0000	0.0198	1100.00	0.0000	defm C-C-C-C, sci C-H
37	1197.92	1180.02	4.0159	0.0000	1102.60	11.601	0.0000	1100.94	23.8030	defm C-C-C-C, sci C-H
38	1197.97	1211.53	0.0000	67.3916	1160.51	0.0000	1252.72	1157.90	0.0000	$\nu C_1 \equiv C_2$ [1.7], sym νC_2-C_3 [4.8], C_1-$C_{3'}$ [4.8]; defm 6 C-C-C [12.2]; defm 8 C-C-H [35.8]
39	1203.48	1211.60	3.6970	0.0000	1184.64	0.0000	25.7537	1179.85	0.0196	sci C-H
40	1226.32	1248.09	0.0000	466.4163	1184.65	0.0132	0.0000	1179.87	0.0000	sci C-H
41	1226.97	1292.38	1.3013	0.0000	1202.17	0.1016	0.0000	1198.01	0.1218	sci C-H, asym sci wrt each other ring
42	1313.71	1293.34	0.0000	35.1037	1203.68	0.0000	61.4909	1198.67	0.0000	sci C-H, sym sci wrt each other ring
43	1314.51	1328.26	0.0000	1.6848	1320.93	0.0000	5.7201	1317.50	0.0000	defm C-C-C, roc C-H
44	1363.26	1329.02	0.9209	0.0000	1324.72	0.0351	0.0000	1321.03	0.7669	defm C-C-C, roc C-H
45	1370.35	1413.28	7.1837	0.0000	1340.38	6.0185	0.0000	1338.13	5.4284	asym νC_2-C_3 [7.7], νC_1-$C_{3'}$ [7.7]; defm<$C_4C_3C_8$ [2.2], <$C_4C_3C_8$ [2]
46	1371.64	1461.19	0.0000	11.8175	1357.49	0.0000	32.6444	1356.31	0.0000	roc {CHs & defm C-C-H [44.9]}; roc wrt each Ph ring
47	1503.06	1463.13	0.6684	0.0000	1357.76	0.6922	0.0000	1356.34	0.8016	roc {CHs & defm C-C-H [48.8]}; sci wrt each Ph ring
48	1559.59	1602.29	0.0000	14.7138	1474.31	0.0000	28.6747	1471.84	0.0000	asym roc (ring edge C-H wrt other ring)
49	1563.14	1604.18	15.584	0.0000	1476.63	7.2784	0.0000	1474.14	11.6921	sym roc (ring edge C-H wrt other ring)

50	1609.20	1655.62	0.0000	63.2437	1519.00	0.0000	235.682	1515.46	0.0000	roc (C-H wrt other ring), νC_1-$C_{3'}$, νC_2-C_3
51	1712.02	1670.11	68.5478	0.0000	1537.42	45.380	0.0000	1533.88	64.9522	roc 4CHs; defm {10 C-C-H [31.4]; defm 2 C-C-C [2.5]}; ν7C-C [13.6]
52	1749.34	1769.81	0.0000	0.1326	1613.27	0.0000	0.6800	1608.58	0.0000	νC-C, roc CHs, sci CHs
53	1752.00	1771.30	3.4305	0.0000	1614.83	2.8887	0.0000	1609.99	4.0187	νC-C, roc CHs, sci CHs
54	1776.51	1801.96	0.0000	1078.5193	1640.83	0.0000	2432.12	1636.66	0.0000	νC_2-C_3 [1.2], νC-C [17.2], defm {C-C-H[25.2], defm C-C-C [7.5]}
55	1797.43	1808.80	25.536	0.0000	1649.75	33.287	0.0000	1645.51	33.5738	νC_2-C_3 [2], νC-C [13.5], defm {C-C-H [25.08], defm C-C-C [4.62]}
56	2494.59	2528.31	0.0000	4610.8433	2301.53	0.0000	9373.64	2295.35	0.0000	$\nu C_1 \equiv C_2$ [36.2], νC_2-C_3 [20.7], νC_1-$C_{3'}$ [20.7]
57	3183.16	3343.01	3.2508	0.0000	3179.92	3.9359	0.0000	3186.41	6.7488	νC-H
58	3183.31	3343.10	0.0000	58.5833	3179.98	0.0000	64.5183	3186.44	0.0000	νC-H
59	3184.99	3353.52	0.0000	262.6738	3188.37	0.0000	311.514	3192.94	0.0000	νC-H
60	3185.21	3353.58	10.782	0.0000	3188.41	11.746	0.0000	3192.96	7.4843	νC-H
61	3189.63	3364.59	58.356	0.0000	3199.47	40.603	0.0000	3202.31	40.3093	νC-H
62	3189.94	3364.70	0.0000	209.2125	3199.56	0.0000	341.066	3202.35	0.0000	νC-H
63	3192.70	3373.25	0.0000	5.8336	3206.97	0.0000	8.2532	3207.90	0.0000	νC-H
64	3193.19	3373.43	62.008	0.0000	3207.17	39.962	0.0000	3207.97	74.3373	asym νC_4-H [13.9], ν C_8-H [13.9]; Asym $\nu C_{4'}$-H [13.9], $\nu C_{8'}$-H [13.9]
65	3201.02	3378.77	27.074	0.0000	3210.99	16.641	0.0000	3213.59	40.4269	νC_4-H [10.1], ν C_8-H [10.1], $\nu C_{4'}$-H [10.1], $\nu C_{8'}$-H [10.1], νC_6-H [7.7], and $\nu C_{6'}$-H [7.7]; 2 ph ring νC-H asym
66	3201.61	3379.00	0.0000	601.6577	3211.18	0.0000	622.280	3213.83	0.0000	νC_4-H [10.1], ν C_8-H [10.1], $\nu C_{4'}$-H [10.1], $\nu C_{8'}$-H [10.1], νC_6-H [7.7], and $\nu C_{6'}$-H [7.7]; 2 ph ring νC-H sym

[a]HF/6-31G(d,p). [b]DFT-B3LYP/6-31+G(d,p) method in gas phase; [c]DFT-B3LYP/6-31+G(d,p) method in ethanol. [d]Unscaled vibrational frequencies in cm^{-1}. [e]Infrared intensities in KM/Mol. [f]Raman scattering activities in A^4/AMU. [g]defm, deformation; tor, torsion; ν, stretching; sym, symmetric; asym, asymmetric; oop, out-of-plane bending; ip, in-plane bending; sci, scissoring; roc, rocking; wag, waging; wrt, with respect to; mode description in DFT-B3LYP/6-31+G(d,p) method in gas phase. [h]For some modes only major contributions of the contribution of internal co-ordinates in percentage (%) are shown.

Conclusion

In the present work, we have calculated the electronic structure, photophysical properties and vibrational frequencies of diphenylacetylene by density functional theory and other theoretical approach. The present UV-Vis spectral analysis by time dependent density functional theory (TD-DFT) method shows that incorporation of solvent shifts the absorption wavelength towards longer wavelength and larger extinction co-efficient. In ethanol solvent the order of the excited state is found as decreased to lower energy level. Raman scattering spectra is found as a useful tool to determine the vibrational spectra for symmetrically substituted acetylene derivative.

References

[1] T. Nomoto, T. Ishibashi, H. Okamoto and M. Hamaguchi, *J. Mol. Struc.*, 2005, 735–736, pp 197–202.

[2] C. Devadoss, P. Bharathi, and J. S. Moore, *J. Am. Chem. Soc.* 1996,118, pp 9635.

[3] M. Shortreed, S. F. Swallen, Z. Shi, W. Tan, Z. Xu, C. Devadoss, J. S. Moore, and R. Kopelman, *J. Phys. Chem. B.* 1997, 101, pp 6318.

[4] R. Kopelman, M. Shortreed, Z. Shi, W. Tan, Z. Xu, J. S. Moore, A. Bar-haim, and J. Klafter, *Phys. Rev. Lett.* 1997, 78, pp 1239 .

[5] J. M. Seminario, A. G. Zacarias, and J. M. Tour, *J. Am. Chem. Soc.* 1998, 120, pp 3970.

[6] J. M. Tour, M. Kozaki, and J. M. Seminario, *J. Am. Chem. Soc.* 1998, 120, pp 8486.

[7] Becke E. D. "Perspective: Fifty years of density-functional theory in chemical physics", *J. Chem. Phys.* 2014, *140*, 18A301, DOI:10.1063/1.4869598.

[8] Gaussian 16, Revision A. 03, M. J. Frisch, G. W. Trucks, H. B. Schlegel, G. E. Scuseria, M. A. Robb, J. R. Cheeseman, G. Scalmani, V. Barone, G. A. Petersson, H. Nakatsuji, X. Li, M. Caricato, A. V. Marenich, J. Bloino, B. G. Janesko, R. Gomperts, B. Mennucci, H. P. Hratchian, J. V. Ortiz, A. F. Izmaylov, J. L. Sonnenberg, D. Williams-Young, F. Ding, F. Lipparini, F. Egidi, J. Goings, B. Peng, A. Petrone, T. Henderson, D. Ranasinghe, V. G. Zakrzewski, J. Gao, N. Rega, G. Zheng, W. Liang, M. Hada, M. Ehara, K. Toyota, R. Fukuda, J. Hasegawa, M. Ishida, T. Nakajima, Y. Honda, O.

Kitao, , H. Nakai, T. Vreven, K. Throssell, J. A. Montgomery, Jr., J. E. Peralta, F. Ogliaro, M. J. Bearpark, J. J. Heyd, N. Brothers, *et. al.*, Gaussian, Inc., Wallingford CT, 2016.

[9] C Lee, W. Yang, and R.G. Parr, *Phys. Rev. B*, 1988, 37, pp 785.

[10] M. J. S. Dewar, E.G. Zoebisch, F. Healy, J. James and P. Stewart, *J. Am. Chem. Soc.* 1985,107 (13), pp 3902.

[11] E. Runge and E. K. U. Gross, Density-functional theory for time-dependent systems, *Phys. Rev. Lett.*, 1984, 52, pp 997-1000.

[12] M. A. Palafox, *Spect. Lett.* 1996, 29 (2), pp 241 – 266.

[13] G. C. Attila, F. Geza, and E. B. James, *J. Phys. Chem.* 1989, 93, pp 7644.

[14] A Shimojima and H. Takahashi, *J. Phys. Chem.* 1993, 97, pp 9103.

[15] A. A. Espiritu and J. G. White, *Z. Krist.,* 1978, 147, pp 177.